We are IntechOpen, the world's leading publisher of Open Access books Built by scientists, for scientists

6,900
Open access books available

186,000
International authors and editors

200M
Downloads

Our authors are among the

154
Countries delivered to

TOP 1%
most cited scientists

12.2%
Contributors from top 500 universities

WEB OF SCIENCE™

Selection of our books indexed in the Book Citation Index in Web of Science™ Core Collection (BKCI)

Interested in publishing with us?
Contact book.department@intechopen.com

Numbers displayed above are based on latest data collected.
For more information visit www.intechopen.com

14

Nonlinear Plasmonics Near the Dirac Point in Negative-Zero-Positive Index Metamaterials –Optical Simulations of Electron in Graphene

Ming Shen and Linxu Ruan
Physics Department, Shanghai University
People's Republic of China

1. Introduction

In 2004, graphene, a single layer of carbon atoms arranged in a hexagonal lattice, has been experimentally realized by A. K. Geim and K. S. Novoselov (Novoselov et al., 2004). In graphene, the conduction and valence bands touch each other at Dirac point (DP) with a double-cone structure (Novoselov et al., 2004). Near DP, the dispersion of electron is linear with two branches (Novoselov et al., 2004). The valence electron dynamics in such a truly two-dimensional (2D) material is governed by a massless Dirac equation. So graphene exhibits many unique electronic properties (Beenakker, 2008; Castro Neto et al., 2009), including half-integer and unconventional quantum Hall effect (Zhang et al., 2005), observation of minimum conductivity (Novoselov et al., 2005), and Klein tunneling (Katsnelson et al., 2006). The optical-like behaviors of electron waves in graphene have also drawn considerable attention recently, such as focusing (Cheianov et al., 2007), collimation (Park et al., 2008a), subwavelength optics (Darancet et al., 2009), Bragg reflection (Ghosh et al., 2009), and Goos-Hänchen effect (Beenakker et al., 2009; Zhao et al., 2010). In this regard, one of the recent work is to investigate the guided modes in monolayer graphene waveguide, by analogy of optical waveguides (Zhang et al., 2009). The exotic properties of the graphene waveguide are found in two different cases of classical motion and Klein tunneing (Zhang et al., 2009). Similar behaviors also happened to the transmission of Dirac-like electron in 2D monolayer graphene barrier at nonzero angle of incidence (Chen and Tao, 2009). The modulation of the transmission gap by the incidence angle, the height, and width of potential barrier may lead to potential applications in graphene-based electronic devices (Chen and Tao, 2009). The electronics waves in graphene can also be treated as the guided waves in an optical fibre, i.e., graphene based electronic fibre (Wu, 2011). The graphene analog of the optical device, the fibre optic, has also been demonstrated both experimentally and numerically in a $p-n$ junction (Williams et al., 2011).

On the other hand, the DP with double-cone structure in photonic crystals (PCs) for the Bloch states is found from the similarity of the photonic bands of the 2D PCs with the electronic bands of solids. Several novel optical transport properties near the DP have been investigated, such as conical diffraction (Peleg et al., 2007), "pseudodiffusive" scaling (Sepkhanov et al., 2007), photon's Zitterbewegung (Zhang, 2008), and perfect Klein tunneling (Bahat-Treidel et al., 2010a). Up to now, the dynamics of Dirac-like excitations in 2D PCs (honeycomb lattices) have been well studied when the propagation equation is linear.

However, the nonlinear dynamics has drawn little attention in the 2D PCs by present. The first study of nonlinear dynamics in honeycomb lattices was conducted in (Peleg et al., 2007), demonstrating gap solitons, which had no overlap with Bloch modes residing in the vicinity of the Dirac points. Subsequently, the nonlinear version of the massless Dirac equation in honeycomb lattices were studied with the Dirac approximation (Ablowitz et al., 2009; Haddad et al., 2009). The nonlinear interactions can also break down the Dirac dynamics in honeycomb photonic lattices (Bahat-Treidel et al., 2010b), open a gap between the first two bands which can support a gap soliton (Bahat-Treidel et al., 2008).

In optical system, Wang *et al.* have shown that, the analogy phenomenon of Dirac point with double-cone structure can be realized in the negative-zero-positive index metamaterial (NZPIM) (Wang et al., 2009a). It is further found that the light field near DP possesses of pseudodiffusive property obeying the $1/L$ scaling law (Wang et al., 2009a). Subsequently, they study the Zitterbewegung of optical pulses near the Dirac point inside a NZPIM (Wang et al., 2009b). The transmission gap, Bragg-like reflection, and Goos-Hänchen shifts near the DP inside a NZPIM slab was further studied comprehensively by Chen *et al.* (Chen et al., 2009). In addition, when the thermal emission frequency is close to the DP, the spectral hemispherical power of thermal emission in layered structures containing NZPIM is strongly suppressed and the emission can become a high directional source with large spatial coherence (Wang et al., 2010). Shen et al. have studied the guided modes in NZPIM waveguide (Shen et al., 2010a), in which the properties of the guided modes are analogous to the propagation of electron waves in graphene waveguide (Zhang et al., 2009). These unique results suggest that many exotic phenomena in graphene can be simulated by the relatively simple optical NZPIM.

Recently, the nonlinear optical response of graphene has been another interesting subject. It has been predicted that the graphene exhibits a strongly nonlinear optical behavior at microwave and terahertz frequencies (Mikhailov, 2007). At higher, optical frequencies one can also expect an enhanced optical nonlinearity as, due to graphene's band structure, interband optical transitions occur at all photon energies. Hendry et al. have performed the first measurements of the coherent nonlinear optical response of single- and few-layer graphene using four-wave mixing (Hendry et al., 2010). Their results demonstrate that graphene exhibits a very strong nonlinear optical response in the near-infrared spectral region. All the results will stimulate much research on the studies of the nonlinear optical response of graphene. Based on the facts of optics-like phenomena of electron wave in graphene and the similarly nonlinear optical dynamics of Dirac equation in 2D PCs, Shen et al. have studied the nonlinear surface waves (Shen et al., 2010b) and the nonlinear guided modes (Shen et al., 2011) near the DP in NZPIM. For the nonlinear NZPIM waveguide, when the nonlinearity is self-focusing, there exists an asymmetric forbidden band near DP which can be modulated by the strength of the nonlinearity. However, the self-defocusing nonlinearity can completely eliminate the asymmetric band gap (Shen et al., 2011).

This chapter presents a review on the propagation of nonlinear plasmonics in NZPIM. The chapter is organized as follow. In Sec. 2, the nonlinear surface wave is discussed at the interface between a nonlinear conventional dielectric media and a linear NZPIM. By analogy of electron wave in monolayer graphene waveguide, the guided modes in NZPIM waveguide is studied in Sec. 3 by the graphic method. In Sec. 4, the nonlinear guided modes are investigated in NZPIM waveguide with a nonlinear dielectric media substrate. Finally, we make brief prospects of the research and conclusion of this chapter in Sec. 5 and 6, respectively.

2. Nonlinear surface waves near the DP in NZPIM

Surface waves, which propagate along the interface between two media and decay in transverse direction, were previously studied at the interface between metal and dielectric medium (Kivshar, 2008). In such systems, the permittivity of the metal is negative and then only the TM-mode surface waves can exist. The TM-mode surface waves can also exist in nonlinear ferromagnetic and antiferromagnetic materials (Wang and Awai, 1998). Surface waves can also propagate in negative refractive metamaterial with simultaneous negative permittivity and negative permeability (Smith et al., 2000). Following the seminal work on the linear TE- and TM-modes surface waves and the nonlinear surface modes in metamaterial (Ruppin, 2000; Shadrivov et al., 2003; 2004), some very recent studies have illustrated that the nonlinear surface wave becomes a more interesting topic from the physical point of view, due to a host of new phenomena in comparison with the linear surface wave. For example, Xu *et. al.* (Xu et al., 2009) have investigated the nonlinear surface polaritons in anisotropic Kerr-type metamaterials. Very lately, we also discovered the bistable and negative lateral shifts in Kretschmann configuration (Chen et al., 2010), where the nonlinear surface waves can be excited at a Kerr nonlinear metamaterial-metal interface.
In this section, we present a comprehensive study of the properties of the nonlinear surface waves at the interface between semi-infinite media of two types, nonlinear conventional dielectric and linear NZPIM, and demonstrate a number of unique properties of surface waves near the DP in a NZPIM.

2.1 Dispersion equation of the nonlinear surface waves

We consider an interface between the nonlinear conventional medium in the $x > 0$ region and the linear NZPIM in the $x < 0$ region. The permittivity and permeability are ϵ_1^{NL} and μ_1 for the nonlinear conventional medium and

$$\epsilon_2(\omega) = 1 - \frac{\omega_{ep}^2}{\omega^2 + i\gamma_e\omega}, \tag{1}$$

$$\mu_2(\omega) = 1 - \frac{\omega_{mp}^2}{\omega^2 + i\gamma_m\omega}, \tag{2}$$

for the NZPIM (Wang et al., 2009a; Ziolkowski, 2004), respectively. ω_{ep}^2 and ω_{mp}^2 are the electronic and magnetic plasma frequencies, and γ_e and γ_m are the damping rates relating to the absorption of the material. Here we assume $\gamma_e = \gamma_m = \gamma \ll \omega_{ep}^2, \omega_{em}^2$. It is important that when $\omega_{ep} = \omega_{em} = \omega_D$ and $\gamma = 0$ (no loss), then $\epsilon_2(\omega) = \mu_2(\omega) = 1 - \omega_D^2/\omega^2$, which indicates both $\epsilon_2(\omega_D)$ and $\mu_2(\omega_D)$ may be zero simultaneously. ω_D is the frequency of the optical DP (corresponding wavelength is $\lambda_D = 2\pi c/\omega_D$), where two bands touch each other forming a double cone structure. In this case, the linear dispersion near the DP, $\omega \approx \omega_D$, can be written as

$$\kappa(\omega) = \frac{\omega - \omega_D}{v_D} = \frac{2(\omega - \omega_D)}{c}, \tag{3}$$

due to the fact that $\kappa(\omega_D) \approx 0$ and $v_D \simeq c/2$ at the DP, where c is the light speed in vacuum. Near the DP, the light transport obeys the massless Dirac equation as follows (Wang et al., 2009a):

$$\begin{bmatrix} 0 & -i(\frac{\partial}{\partial x} - i\frac{\partial}{\partial y}) \\ -i(\frac{\partial}{\partial x} + i\frac{\partial}{\partial y}) & 0 \end{bmatrix} \Psi = \left(\frac{\omega - \omega_D}{v_D}\right) \Psi, \tag{4}$$

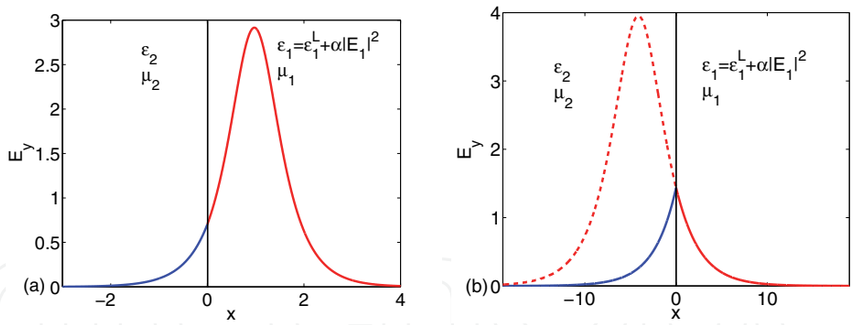

Fig. 1. (Color online). The transverse profile of the nonlinear surface waves: (a) $\mu_2 > 0$ and (b) $\mu_2 < 0$.

where $\Psi = \begin{pmatrix} E_{z1}(x,y,\omega) \\ E_{z2}(x,y,\omega) \end{pmatrix}$ are the eigenfunctions of the electric fields with the same $k(\omega)$. We consider the TE-mode electric field in this paper, and the propagation of the surface waves obey the following nonlinear differential equations

$$\frac{\partial^2 E_y}{\partial x^2} - (\kappa^2 - \kappa_0^2 \epsilon_1^{NL} \mu_1) E_y = 0, x > 0, \tag{5}$$

$$\frac{\partial^2 E_y}{\partial x^2} - \kappa_2^2 E_y = 0, x < 0, \tag{6}$$

where $\kappa_0 = \omega/c$ is the wave vector in vacuum, $\epsilon_1^{NL} = \epsilon_1^L + \alpha |E_1|^2$, ϵ_1^L is the linear permittivity and α is the nonlinear index of medium 1, κ is the propagation constant of the nonlinear surface wave, and $\kappa_1^2 = \kappa^2 - \kappa_0^2 \epsilon_1^L \mu_1$ and $\kappa_2^2 = \kappa^2 - [2(\omega - \omega_D)/c]^2$ are the decay constants in nonlinear medium and NZPIM, respectively. We only consider a self-focusing nonlinearity with $\alpha > 0$. It should be strengthened that for the self-defocusing nonlinearity $\alpha < 0$, the transverse electronic field will very different from the case of self-focusing nonlinearity. The solution of Eqs. (5) and (6) have the following form

$$E_{1y} = \frac{\kappa_1}{\kappa_0} \sqrt{\frac{2}{\alpha \mu_1}} sech[\kappa_1 (x - x_0)], x > 0, \tag{7}$$

$$E_{2y} = E_2 \exp(\kappa_2 x), x < 0. \tag{8}$$

Applying the continuity of wave function at the interface $x = 0$, we obtain two equations as follow

$$E_2 = \frac{\kappa_1}{\kappa_0} \sqrt{\frac{2}{\alpha \mu_1}} sech(\kappa_1 x_0), \tag{9}$$

$$\frac{\kappa_2}{\mu_2} E_2 = \frac{\kappa_1^2}{\mu_1 \kappa_0} \sqrt{\frac{2}{\alpha \mu_1}} \frac{\tanh(\kappa_1 x_0)}{\cosh(\kappa_1 x_0)}, \tag{10}$$

which yields

$$\tanh(\kappa_1 x_0) = \frac{\mu_1 \kappa_2}{\mu_2 \kappa_1}, \tag{11}$$

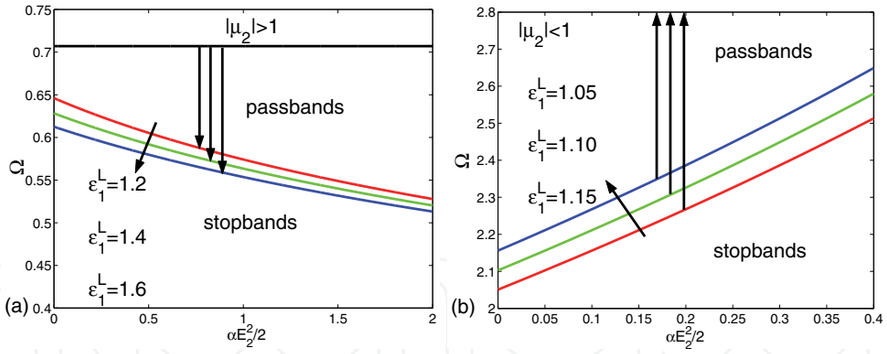

Fig. 2. (Color online). Variation of Ω with $\alpha E_2^2/2$, for three different value ϵ_1^L when (a) $|\mu_2| > 1$ ($\mu_2 < 0$) and (b) $|\mu_2| < 1$ ($\mu_2 > 0$).

and the dispersion equation

$$\frac{\kappa^2}{\kappa_0^2} = \frac{\mu_1}{\mu_2^2 - \mu_1^2}\left[\mu_2^2\epsilon_1^L + \frac{\mu_2^2\alpha E_2^2}{2} - 4\mu_1(1-\frac{\omega_D}{\omega})^2\right]. \tag{12}$$

From Eq. (11), we know that the transverse profile of the nonlinear surface waves depend on the sign of μ_2. The maximum of the dielectric fields amplitude are located at the interface when $\mu_2 < 0$ and located inside the nonlinear dielectric medium when $\mu_2 > 0$, as shown in Fig. 1.

The power fluxes is described by the Poynting vector $P = 1/2\int(\vec{E}\times\vec{H}^*)_z dx = P^{NL} + P^L$ with

$$P^{NL} = \frac{\kappa\kappa_1}{\mu_0\mu_1^2\kappa_0^2\omega\alpha}\left(1+\frac{\mu_1\kappa_2}{\mu_2\kappa_1}\right), \tag{13}$$

$$P^L = \frac{\kappa\kappa_1^2}{2\mu_0\mu_1\mu_2\kappa_2\kappa_0^2\omega\alpha}\left[1-\left(\frac{\mu_1\kappa_2}{\mu_2\kappa_1}\right)^2\right], \tag{14}$$

are the power fluxes in the nonlinear medium and NZPIM, respectively.

The dispersion equation Eq. (12) tells us that increasing αE_2^2 will reduce or increase the effective wave index κ/κ_0. For the surface waves, the propagation constant should be larger than wave vector in the nonlinear medium and NZPIM

$$\kappa^2 > \kappa_0^2\epsilon_1^L\mu_1, \kappa^2 > \left[\frac{2(\omega-\omega_D)}{c}\right]^2 = 4\kappa_0^2(1-\frac{\omega_D}{\omega})^2. \tag{15}$$

Define a parameter $\Omega = \omega/\omega_D$, and then the permittivity and the permeability of NZPIM are $\epsilon_2 = \mu_2 = 1 - 1/\Omega^2$. Eq. (12) also gives the following necessary conditions for the nonlinear surface wave existence, since κ^2/κ_0^2 should be positive:

$$\mu_2^2\epsilon_1^L + \frac{\mu_2^2\alpha E_2^2}{2} - 4\mu_1(1-\frac{\omega_D}{\omega})^2 < 0, (|\mu_2| < \mu_1), \tag{16}$$

$$\mu_2^2\epsilon_1^L + \frac{\mu_2^2\alpha E_2^2}{2} - 4\mu_1(1-\frac{\omega_D}{\omega})^2 > 0, (|\mu_2| > \mu_1). \tag{17}$$

In the next, we will study the nonlinear surface waves in NZPIM when $|\mu_2| < \mu_1$ and $|\mu_2| > \mu_1$, respectively.

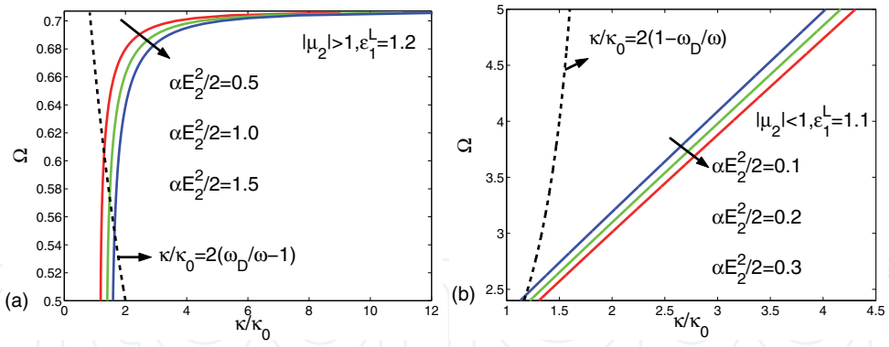

Fig. 3. (Color online). Dispersion relation of Ω versus normalized propagation constant, for three different $\alpha E_2^2/2$ when (a) $|\mu_2| > 1$ and (b) $|\mu_2| < 1$.

2.2 Pass and stop bands, power fluxes, and group velocity of the nonlinear surface waves

Case A: $|\mu_2| < \mu_1$. From the Eqs. (15) and (16), we obtain the following condition for the surface propagation:

$$\epsilon_1^L < 4(1 - \frac{1}{\Omega})^2 - \frac{\alpha E_2^2}{2}. \tag{18}$$

For simplicity, we assume that $\mu_1 = 1$ in this article. Since $|\mu_2| < 1$, Ω obeys $\sqrt{2}/2 < \Omega < 1$ or $\Omega > 1$. We rewrite Eq. (18) as

$$A\Omega^2 + B\Omega + C > 0, \tag{19}$$

where $A = 4 - (\epsilon_1^L + \frac{\alpha E_2^2}{2})$, $B = -8$, $C = 4$, and $a = \epsilon_1^L + \frac{\alpha E_2^2}{2} > 1$ for general dielectric medium. The solution of Eq. (19) is

$$\Omega > \frac{4 + 2\sqrt{a}}{4 - a}, 1 < a < 4. \tag{20}$$

Case B: $|\mu_2| > \mu_1$. From the Eqs. (15) and (17), we obtain that

$$\epsilon_1^L > 4(1 - \frac{1}{\Omega})^2 - \frac{\alpha E_2^2}{2}. \tag{21}$$

Since $|\mu_2| > 1$, Ω obeys $0 < \Omega < \sqrt{2}/2$. Similarly, we can get the solution of Eq. (21)

$$\frac{4 - 2\sqrt{a}}{4 - a} < \Omega < \frac{\sqrt{2}}{2}, a > 1. \tag{22}$$

From Eqs. (20) and (22), we know that there is a forbidden band near the optical dirac point for the nonliear surface waves. For $\sqrt{2}/2 < \Omega < 2$, the nonlinear surface wave do not exist. The existence regions of the nonlinear surface waves also depend on the frequency properties and the nonlinear value $\alpha E_2^2/2$, i.e., the passbands and stopbands, as shown in Fig. 2. It is shown that when $|\mu_2| > 1$ ($\mu_2 < 0$) the passbands of the surface waves have a maximum frequency limit $\sqrt{2}/2\omega_D$. The increase of the nonlinear part $\alpha E_2^2/2$ reduces the lower frequency limit Ω and widens the passband, as shown in Fig. 2 (a). From Fig. 2 (b), we know that, the passbands have a minimum frequency limit, and the increase of the nonlinear part $\alpha E_2^2/2$ increases the minimum frequency limit and reduces the passbands when $|\mu_2| < 1$ ($\mu_2 > 0$). For that the value of the nonlinear part $\alpha E_2^2/2$ can be modulated by increasing or decreasing the power, so

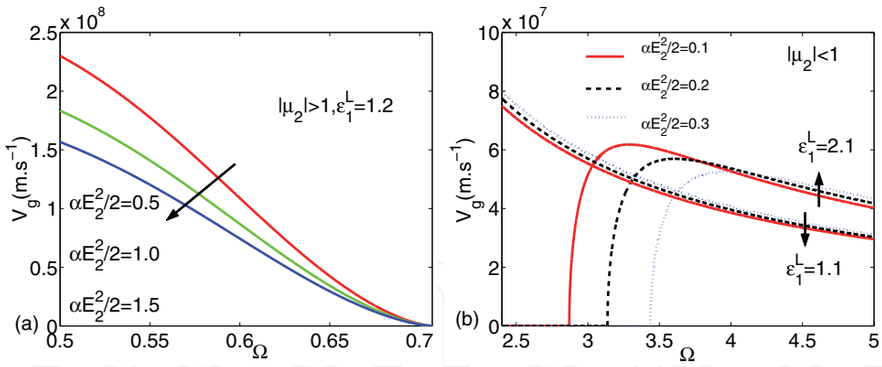

Fig. 4. (Color online). Group velocity V_g versus normalized frequency, for three different $\alpha E_2^2/2$ when (a) $|\mu_2| > 1$ and (b) $|\mu_2| < 1$.

it maybe have potential applications in optical devices and guided wave optics.

In Fig. 3, we plot the frequency dispersion of the nonlinear surface waves. We find that the normalized propagation constants will increase when the normalized frequency increase for both $\mu_2 > 0$ and $\mu_2 < 0$. The dispersion curves are always positive in the existence regions which means the nonlinear surface waves are always forward with a positive power fluxes. This is very different from the frequency dispersion in left-hand materials, whereas the dispersion curves may be negative under some conditions (Shadrivov et al., 2004). Fig. 3 also shows that the dispersion curves have a maximum (minimum) limit for the parameter Ω when $|\mu_2| > 1$ ($|\mu_2| < 1$), which corresponding to the forbidden bands described in Fig. 2. As to the case $|\mu_2| > 1$ (negative index), we can see the upper limit for the parameter Ω is $\Omega = \sqrt{2}/2$.

Group velocity is an important parameter for the propagation of the surface waves. It can describe the direction of the power fluxes. We rewrite dispersion relation Eq. (12) as

$$\kappa = \kappa_0 \left\{ \frac{\mu_1}{\mu_2^2 - \mu_1^2} \left[\mu_2^2 \epsilon_1^L + \frac{\mu_2^2 \alpha E_2^2}{2} - 4\mu_1 (1 - \frac{\omega_D}{\omega})^2 \right] \right\}^{1/2}, \tag{23}$$

which yields that

$$\frac{d\kappa}{d\omega} = \frac{\kappa}{\omega} + \frac{\kappa_0^2}{2\kappa} \{ (\frac{\mu_1}{\mu_2^2 - \mu_1^2})' [\mu_2^2 \epsilon_1^L + \frac{\mu_2^2 \alpha E_2^2}{2} - 4\mu_1 (1 - \frac{\omega_D}{\omega})^2] + \frac{\mu_1}{\mu_2^2 - \mu_1^2} [(2\epsilon_1^L + \alpha E_2^2)\mu_2 \mu_2' - 8\mu_1 (1 - \frac{\omega_D}{\omega})(1 - \frac{\omega_D}{\omega})'] \}, \tag{24}$$

where $(\frac{\mu_1}{\mu_2^2 - \mu_1^2})' = -\frac{2\mu_1 \mu_2 \mu_2'}{(\mu_2^2 - \mu_1^2)^2}$, $\mu_2' = 2\omega_D^2/\omega^3$, and $(1 - \frac{\omega_D}{\omega})' = \omega_D/\omega^2$. The group velocity can be represented as

$$V_g = d\omega/d\kappa = (d\kappa/d\omega)^{-1}. \tag{25}$$

In Fig. 4, we plot the group velocity of the nonlinear surface wave in two different conditions $|\mu_2| > 1$ and $|\mu_2| < 1$. We know that the group velocity of the nonlinear surface waves is always positive which means the power fluxes is always positive and the surface waves are always forward. When $\mu_2 < 0$, the group velocity will decrease when the frequency increase.

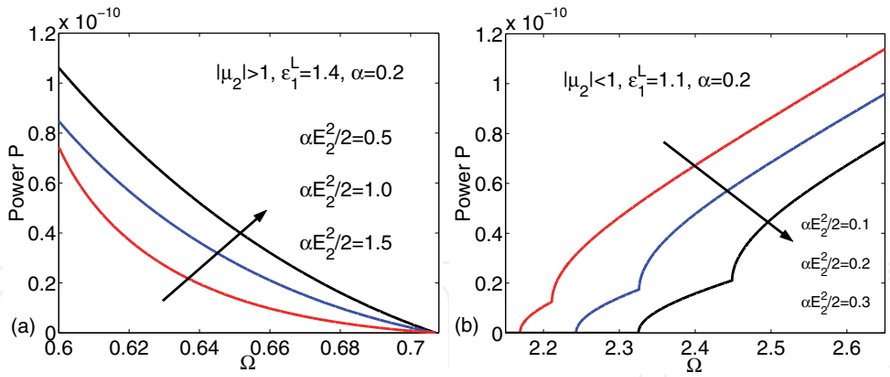

Fig. 5. (Color online). Total power versus normalized frequency, for three different $\alpha E_2^2/2$ when (a) $|\mu_2| > 1$ and (b) $|\mu_2| < 1$.

It will reach zero at the point $\omega = \sqrt{2}/2\omega_D$, which means the nonlinear surface waves is forbidden at this point. When $\omega = \sqrt{2}/2\omega_D$, $|\mu_2| = \mu_1 = 1$ ($\mu_2 = -1$), we have $\kappa \to \infty$ and the nonlinear surface wave stops. The group velocity will decrease when the nonlinear part $\alpha E_2^2/2$ increase. However, they will all stop at the point $\omega = \sqrt{2}/2\omega_D$, as shown in Fig. 4 (a). Fig. 4 (b) shows that the group velocity has a lower frequency limit for a given ϵ_1^L and the nonlinear part $\alpha E_2^2/2$ when $|\mu_2| < 1$. This lower frequency limit imply a power threshold of the surface waves. The lower frequency limit will increase when the linear permittivity of ϵ_1^L or the nonlinear part $\alpha E_2^2/2$ increase. This result can also be obtained from Fig. 2 (b), the passbands have a minimum frequency limit, and the increase of the nonlinear part $\alpha E_2^2/2$ increases the minimum frequency limit and reduces the passbands. We also find the group velocity will increase firstly and then decrease when it reaches the maximum. The group velocity is always positive when $\mu_2 < 0$ which means the nonlinear surface waves are always forward with positive power fluxes.

We also plot the power fluxes of the nonlinear surface waves in Fig. 5 by calculating Eqs. (13) and (14). It is shown that the power flux will approximately linear decrease near the Dirac point when $\mu_2 < 0$, as shown in Fig. 5 (a). And the power flux will be zero when $\omega = \sqrt{2}/2\omega_D$ for that the nonlinear surface waves stops at this point. We also find that increase the nonlinear part $\alpha E_2^2/2$ can effectively increase the power fluxes of the nonlinear surface waves when the frequency is near the Dirac point. When $\mu_2 > 0$, from Fig. 5 (b) we can see that the power fluxes have a frequency threshold for a given ϵ_1^L and the nonlinear part $\alpha E_2^2/2$. This threshold will increase when the nonlinear part $\alpha E_2^2/2$ increase, and this result also shown in Fig. 4 (b). The power flux will also increase when the frequency increase. However, the power fluxes will decrease when the nonlinear part $\alpha E_2^2/2$ increase for the same frequency.

3. Guide modes in NZPIM waveguide

In 2009, Zhang et al. have investigated the guided modes in monolayer graphene waveguide, by analogy of optical waveguides (Zhang et al., 2009). In this section, we will investigate systemically the guided modes in NZPIM waveguide by using the graphic method. For the fast wave guided modes, it is shown that the fundamental mode is absent when the angular frequency is smaller than the DP. Whereas the NZPIM waveguide behaves like conventional dielectric waveguide, when the angular frequency is larger than the DP. The unique properties

of the guided modes are very similar as the propagation of electronic wave in graphene waveguide, corresponding to the classical motion and the Klein tunneling Zhang et al. (2009).

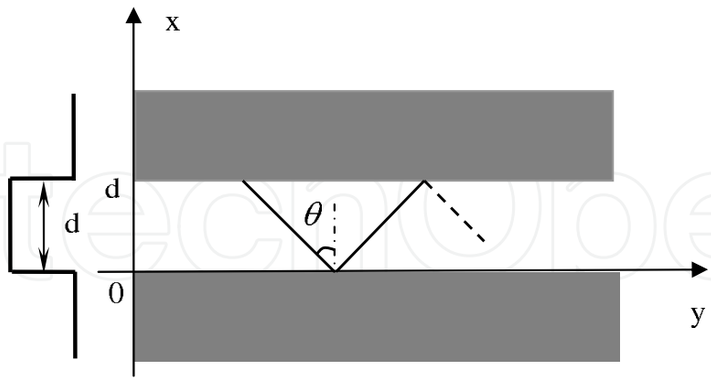

Fig. 6. Schematic structure of negative-zero-positive index metamaterial (NZPIM) waveguide, where the core is the air with the thickness is d and the cladding is the so-called NZPIM.

3.1 Model and basic equation

We consider a waveguide structure of NZPIM, as shown in Fig. 6, where the core is the air with the thickness is d and the cladding is the so-called NZPIM, the optical wave with angle θ is incident upon the waveguide, the direction of the guide modes is z axis, and there are two types of situations: (a) when the incident angle is less than the total internal reflection (TIR) angle, the modes become radiation modes; (b) if the incident angle is more than the critical angle, there will exist oscillating guided modes. What as follows we will focus on the latter case. The TIR angle is defined by $\sin\theta_c = \kappa_2/\kappa_1$, where $\kappa_1 = \omega/c$ is the wavevector in the air, and $\kappa_2 = (\omega - \omega_D)/v_D$ is the wave vector of the NZPIM near the DP (Wang et al., 2009a).
We consider the transverse electric (TE) guided modes [TM modes can be obtained in the same way], the electric fields in the three regions can be written as

$$\psi_A(x) = \begin{cases} Ae^{\alpha x}e^{i\beta y}, & x < 0, \\ [B\cos(\kappa_x x) + C\sin(\kappa_x x)]\, e^{i\beta y}, & 0 < x < d, \\ De^{-\alpha(x-d)}e^{i\beta y}, & x > d, \end{cases} \tag{26}$$

where $\kappa_x = \kappa_1\cos\theta$, $\beta = \kappa_1\sin\theta$ is the propagation constant of the guide modes, and $\alpha = \sqrt{\beta^2 - \kappa_2^2}$ is the decay constant in the cladding region.
Applying the continuity of wave function at the interface $x = 0$ and $x = d$, we obtain the corresponding dispersion equation as follow:

$$\tan(\kappa_x d) = \frac{2\mu_1\mu_2\alpha\kappa_x}{\mu_2^2\kappa_x^2 - \mu_1^2\alpha^2}. \tag{27}$$

We make Eq. (27) in dimensionless form

$$F(\kappa_x d) = \frac{2\mu_1\mu_2(\kappa_x d)\sqrt{(\kappa_1 d)^2 - (\kappa_x d)^2 - (\kappa_2 d)^2}}{\mu_2^2(\kappa_x d)^2 - \mu_1^2[(\kappa_1 d)^2 - (\kappa_x d)^2 - (\kappa_2 d)^2]}. \tag{28}$$

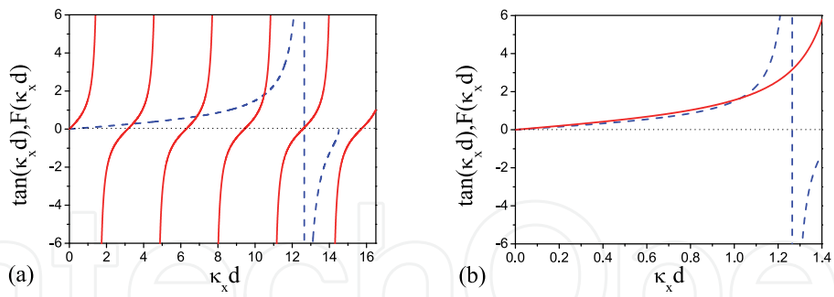

Fig. 7. (Color online). Graphical determination of $\kappa_x d$ for fast wave guided modes when $w < w_D$. The solid and dashed curves correspond to tan $(\kappa_x d)$ and $F(\kappa_x d)$, respectively. The initial parameters are $\omega_D = 2\pi \times 10GHz$, $\omega = 0.8\omega_D$ which means the total reflection angle is $\theta_c = 30^\circ$, the thickness of the core are (a) $d = 10cm$ and (b) $d = 1cm$.

The dispersion Eq. (28) is a transcendental one and cannot be solved analytically, so we propose a graphical method to determine the solution of $\kappa_x d$ for the guided modes. We will discuss the properties of the guided modes in two cases $\omega < \omega_D$ and $\omega > \omega_D$, respectively.

3.2 Fast wave guided modes

Case 1: $\omega < \omega_D$. The critical angle is defined as

$$\theta_c = \sin^{-1}\left[2\left(\frac{\omega_D}{\omega} - 1\right)\right] \tag{29}$$

with the necessary condition $\frac{2}{3}\omega_D < \omega < \omega_D$ (Chen et al., 2009).
As shown in Fig. 7 (a), we plot the dependencies of $\tan(\kappa_x d)$ and $F(\kappa_x d)$ on $\kappa_x d$. The intersections show the existence of the guided modes, as shown in Fig. 8 (a), (b), and (c), corresponding to the TE_2, TE_3, and TE_4 modes, respectively. We find that for some waveguide parameters, the lower-order mode TE_1 can not coexist with higher-order guided modes. So we can not solve TE_1 mode in the same graph Fig 7 (a). This is because that the waveguide parameters used in Fig. 7 (a) does not satisfy the dispersion relation of Eq. (30) when $m = 1$. We can reduce the thickness of the waveguide to obtain the TE_1 mode in the NZPIM waveguide, as shown in Fig. 8 (d), which corresponds to the dispersion relation graphic of Fig 7 (b) with the waveguide thickness is $d = 1cm$.
Another interesting property of the guided modes is that the absence of fundamental TE_0 mode for any parameters of the NZPIM waveguide, which is a novel property different from that in conventional waveguide. The unique property is similar as the guide modes of electron waves in graphene waveguide, where the fundamental mode is absent in the Klein tunneling case (Zhang et al., 2009). For the TE modes, we can write the dispersion relation Eq. (27) as

$$\kappa_x d = m\pi + 2\phi, m = 0, 1, 2, ... \tag{30}$$

where

$$\phi = \arctan\left(\frac{\mu_1 \alpha}{\mu_2 \kappa_x}\right), \tag{31}$$

is negative (angular frequency is smaller than the Dirac point, $\mu_2 < 0$, corresponding Klein tunneling in graphene), which represents the phase retardation upon the total internal reflection at the interface between air and the NZPIM. From Eq. (30), we know that for the

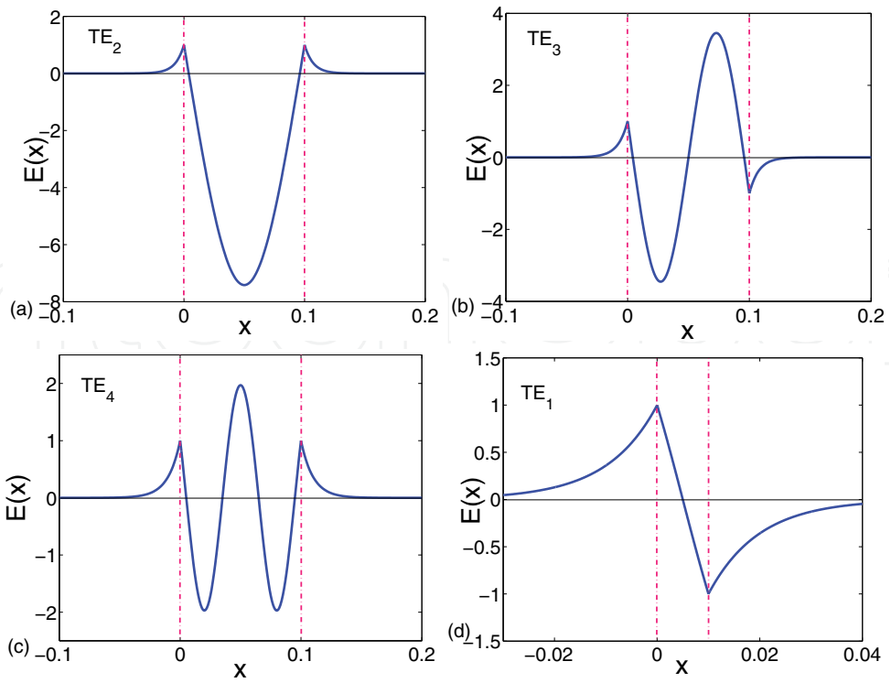

Fig. 8. (Color online) The wave function of guided modes as a function of distance of NZPIM waveguide corresponding to the intersection in Fig. 7 when $\omega < \omega_D$. (a) TE_2: $\kappa_x d = 3.41$; (b) TE_3: $\kappa_x d = 6.87$; (c) TE_4: $\kappa_x d = 10.49$; (d) TE_1: $\kappa_x d = 1.03$.

fundamental mode ($m = 0$), it does not meet with the required dispersion relation. In fact, the condition for the guided waves to exist in a slab waveguide, has a simple physical meaning: the round-trip accumulation of phase due to wave propagation across the layer, $2\phi_{prop}$, including the phase retardation upon the total internal reflection, $2\phi_{refl}$, should be equal to a multiple of 2π (Shadrivov et al., 2005). When the angular frequency is smaller than the Dirac point (the permittivity and the permeability are both negative, NZPIM can be treated as left-handed material), the total phase change does not satisfy the required dispersion relation of Eq. (30), and no fundamental guided modes exist (Shadrivov et al., 2003; 2005). This result is also shown in Fig. (11), where we plot the propagation constant of the guided modes as a function of incident frequency near the DP. It is obviously that the dispersion of TE_0 mode only exist when $\omega > \omega_D$.

Case 2: $\omega > \omega_D$. The critical angle is defined as

$$\theta_c = \sin^{-1}\left[2\left(1 - \frac{\omega_D}{\omega}\right)\right] \tag{32}$$

with the necessary condition $\omega_D < \omega < 2\omega_D$ (Chen et al., 2009). Similarly, we obtain the guided modes of the NZPIM waveguide by using the graphical method, as shown in Fig. 9. It is shown that when $\omega > \omega_D$, the properties of the NZPIM waveguide can be treated as a conventional dielectric waveguide. From Fig. 10, we can see that the fundamental odd and even guided modes can coexist with higher-order modes within the same waveguide for general parameters, which is very different from the case when $\omega < \omega_D$. Under this condition, it corresponds to the guided modes in graphene waveguide in classical motion (Zhang et al., 2009).

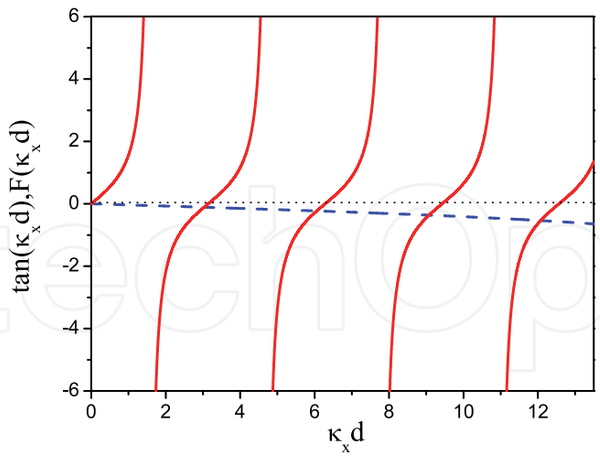

Fig. 9. (Color online) Graphical determination of $\kappa_x d$ for fast wave guided modes when $\omega > \omega_D$. The solid and dashed curves correspond to tan $(\kappa_x d)$ and $F(\kappa_x d)$, respectively. The initial parameters are $\omega_D = 2\pi \times 10GHz$, $\omega = 4\omega_D/3$ which means the total reflection angle is $\theta_c = 30°$, the thickness of the core is $d = 10cm$.

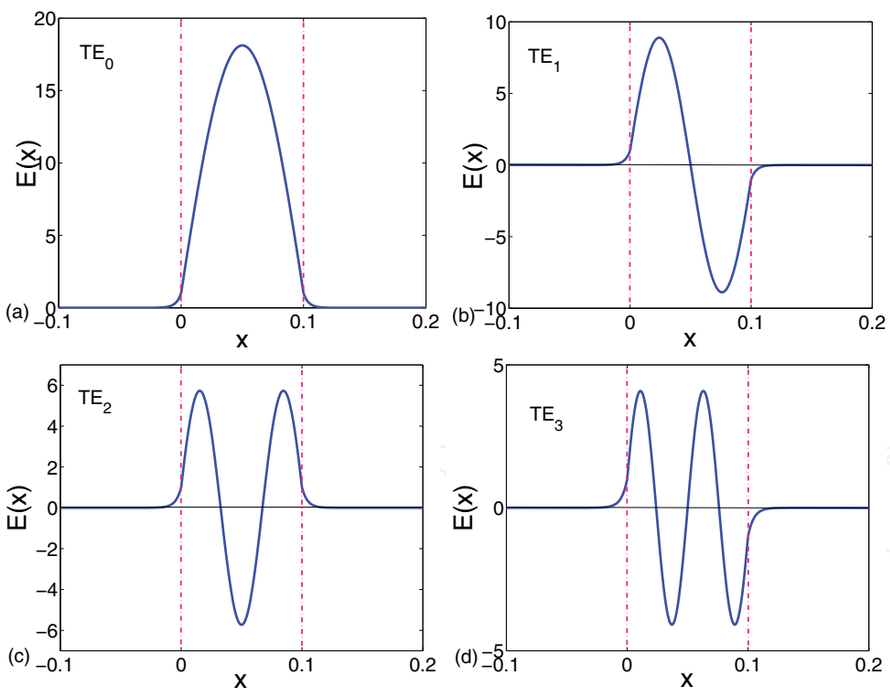

Fig. 10. (Color online) The wave function of guided modes as a function of distance of NZPIM waveguide corresponding to the intersection in Fig. 9 when $\omega > \omega_D$. (a) TE_0: $\kappa_x d = 3.03$; (b) TE_1: $\kappa_x d = 6.06$; (c) TE_2: $\kappa_x d = 9.07$; (d) TE_3: $\kappa_x d = 12.07$.

In order to show further the unique properties of guides modes near the DP in NZPIM waveguides, we plot the dispersion of the guided modes when the incident frequency varies

from $\omega < \omega_D$ to $\omega > \omega_D$ in Fig. 11. As discussed above, we can see that TE_0 mode only exist when $\omega > \omega_D$. In addition, another important and interesting property of the guided modes is that there exists an asymmetric forbidden band for the dispersion. The band will also become wider when the order of the guided modes increases with increasing the incidence angle. The result indicates that the modes are not continuous near the DP. This behavior on the forbidden band discussed here is very similar to the transmission gap in the NZPIM slab (Chen et al., 2009). It seems that the guided modes near the DP are quite different from the negative refractive index metamaterial waveguides discussed in Ref. (Shadrivov et al., 2003), though one can divide NZPIM two parts with positive index and negative index respectively by DP, which corresponds to $\omega > \omega_D$ and $\omega < \omega_D$.

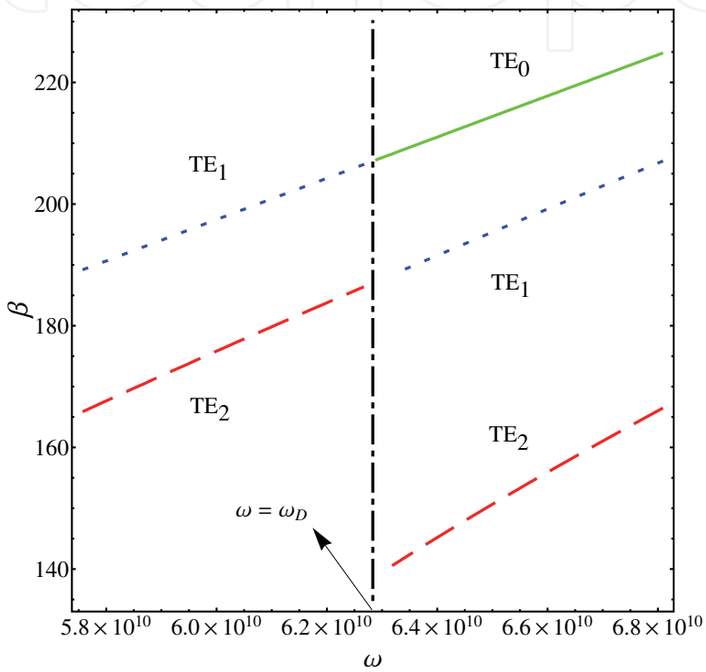

Fig. 11. (Color online) The propagation constant β versus the incident frequency ω near the DP in the NZPIM waveguide.

3.3 Slow wave guided modes

We also find that when $\omega < \omega_D$, the NZPIM waveguide can propagate surface guided modes-slow wave. In this case, the function of the modes in core become sinh and cosh with the imaginary transverse κ_x, and the electric fields in three regions can be written as

$$\psi_A(x) = \begin{cases} Ae^{\alpha x}e^{i\beta y}, & x < 0, \\ [B\cosh(\kappa_x x) + C\sinh(\kappa_x x)]\, e^{i\beta y}, & 0 < x < d, \\ De^{-\alpha(x-d)}e^{i\beta y}, & x > d, \end{cases} \tag{33}$$

where κ_x is the transverse decay constant in the core region, and $\beta^2 = \kappa_1^2 + \kappa_x^2$ is the propagation constant of the slow wave guided modes, and $\alpha = \sqrt{\beta^2 - \kappa_2^2}$ is the decay constant in the cladding region.

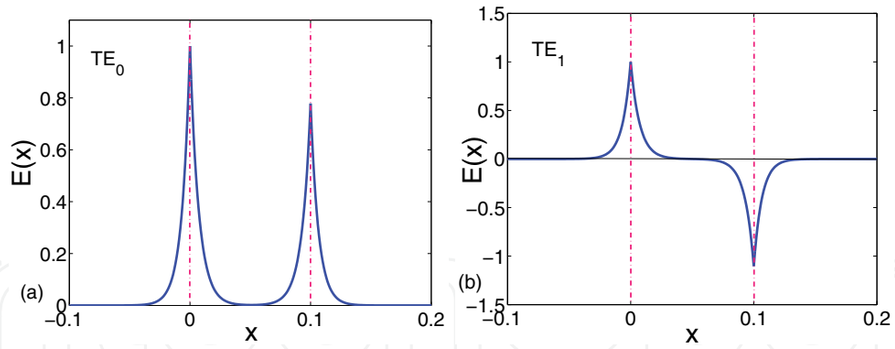

Fig. 12. (Color online). The wave function of guided modes as a function of distance of NZPIM waveguide. The initial parameters are $\omega_D = 2\pi \times 10GHz$, $\omega = 0.69\omega_D$, and the thickness of the core is $d = 10cm$.(a) TE_0: $\kappa_x d = 13.8109$; (b) TE_1: $\kappa_x d = 13.8112$.

Similarly, we obtain the corresponding dispersion equation of this system

$$\tanh(\kappa_x d) = -\frac{2\mu_1\mu_2\alpha\kappa_x}{\mu_2^2\kappa_x^2 + \mu_1^2\alpha^2}. \tag{34}$$

Write Eq. (34) in dimensionless form as follow

$$F(\kappa_x d) = -\frac{2\mu_1\mu_2(\kappa_x d)\sqrt{(\kappa_1 d)^2 + (\kappa_x d)^2 - (\kappa_2 d)^2}}{\mu_2^2(\kappa_x d)^2 + \mu_1^2[(\kappa_1 d)^2 + (\kappa_x d)^2 - (\kappa_2 d)^2]}. \tag{35}$$

As discussed above, we also propose a graphical method to solve the surface guided modes. We find that only fundamental odd and even surface guided modes can exist in the waveguide for some parameters. As shown in Fig. 12, higher-order surface modes are forbidden except the TE_0 and TE_1 surface guided modes. These results obtained here also predict the surface mode of electrons and holes in graphene waveguide.

We emphasize that these results discussed here do extend the investigations (Shadrivov et al., 2003; 2005) and applications (Tsakmakidis et al., 2007) of the waveguide containing only left-handed material. On one hand, we can control the properties of guides modes for the potential applications by adjusting the angular frequency with respect to the DP. On the other hand, our work will also motivate the further work to simulate many exotic phenomena in graphene with relatively simple optical benchtop experiments, based on the links between Klein paradox and negative refraction (Güney and Meyer, 2009).

4. Tunable band gap near the Dirac point in nonlinear negative-zero-positive index metamaterial waveguide

The optical-like behaviors of electron waves in graphene have also drawn considerable attention recently, for example, graphene based electronic fibre and waveguide. In Sec. 3, we have studied the guided modes in NZPIM waveguide (Shen et al., 2010a), in which the properties of the guided modes are analogous to the propagation of electron waves in graphene waveguide (Zhang et al., 2009). However, the nonlinearity may affect the properties of guided modes near the DP in a special manner. In this section, we investigate systemically the guided modes in nonlinear NZPIM waveguide. When the nonlinearity is self-focusing, there exists an asymmetric forbidden band near DP which can be modulated by the strength of the nonlinearity. However, the self-defocusing nonlinearity can completely eliminate the asymmetric band gap.

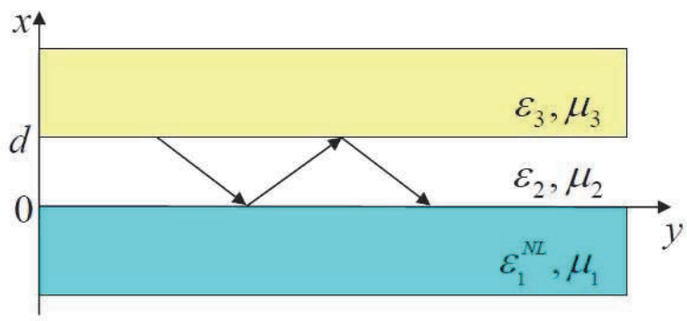

Fig. 13. (Color online) Schematic structure of the NZPIM waveguide with a nonlinear substrate, the core thickness is d.

4.1 Model and basic equation

Considering a nonlinear NZPIM waveguide structure, as shown in Fig. 13. The core of the waveguide is conventional dielectric medium with the thickness d, the permittivity and the permeability are ϵ_2 and μ_2. The substrate is the nonlinear medium with the permittivity and the permeability are $\epsilon_1^{NL} = \epsilon_1^L + \alpha|E_1|^2$ and μ_1, where ϵ_1^L is the linear refractive index and α is the nonlinear coefficient index, $\alpha > 0$ ($\alpha < 0$) corresponding to self-focusing (self-defocusing) nonlinearity. The cladding is NZPIM with the permittivity and the permeability are $\epsilon_3 = \mu_3 = 1 - \omega_D^2/\omega^2$ (Shen et al., 2010a; Wang et al., 2009a).

We only consider the transverse electric (TE) nonlinear guided modes. When the substrate has a self-focusing nonlinearity $\alpha > 0$, the electric fields in three regions can be written as

$$\psi(x) = \begin{cases} \frac{k_1}{k_0}\sqrt{\frac{2}{\alpha\mu_1}}\mathrm{sech}[k_1(x - x_0)], & x < 0, \\ Ae^{ik_2(x-d)} + Be^{-ik_2(x-d)}, & 0 < x < d, \\ Ce^{-k_3(x-d)}, & x > d, \end{cases} \tag{36}$$

where $k_1^2 = \beta^2 - k_0^2\epsilon_1^L\mu_1$ and $k_3^2 = \beta^2 - [2(\omega - \omega_D)/c]^2$ are the transverse decay indexes in substrate and cladding, $k_2^2 = k_0^2\epsilon_2\mu_2 - \beta^2$ is the transverse wave vector of the guided modes in core and it is real, β is the propagation constant of the nonlinear fast wave guide modes. For convenience, we assume the nonlinear substrate and the core are non-magnetic medium with $\mu_1 = \mu_2 = 1$.

Applying the continuity of wave function at the interfaces $x = 0$ and $x = d$, we obtain the corresponding dispersion equation as follow:

$$\tan(k_2 d) = \frac{\mu_1\mu_2 k_2 k_3 - \mu_2\mu_3 k_1 k_2 \tanh(-k_1 x_0)}{\mu_1\mu_3 k_2^2 + \mu_2^2 k_1 k_3 \tanh(-k_1 x_0)}, \tag{37}$$

where $x_0 = -\frac{1}{k_1}\mathrm{sech}^{-1}\left[\frac{k_0}{k_1}\sqrt{\frac{\alpha\mu_1}{2}}(\cos k_2 d + \frac{\mu_2 k_3}{\mu_3 k_2}\sin k_2 d)C\right]$ is the position of the maximum of the amplitude in nonlinear substrate, C being the amplitude of the electric field at the interface $x = d$. In the whole paper, we make the assumption $C = 1$. Next, we will discuss the properties of the nonlinear guided modes by using the graphic method (Shen et al., 2010a; Zhang et al., 2009) near DP in two cases $\omega < \omega_D$ and $\omega > \omega_D$, respectively.

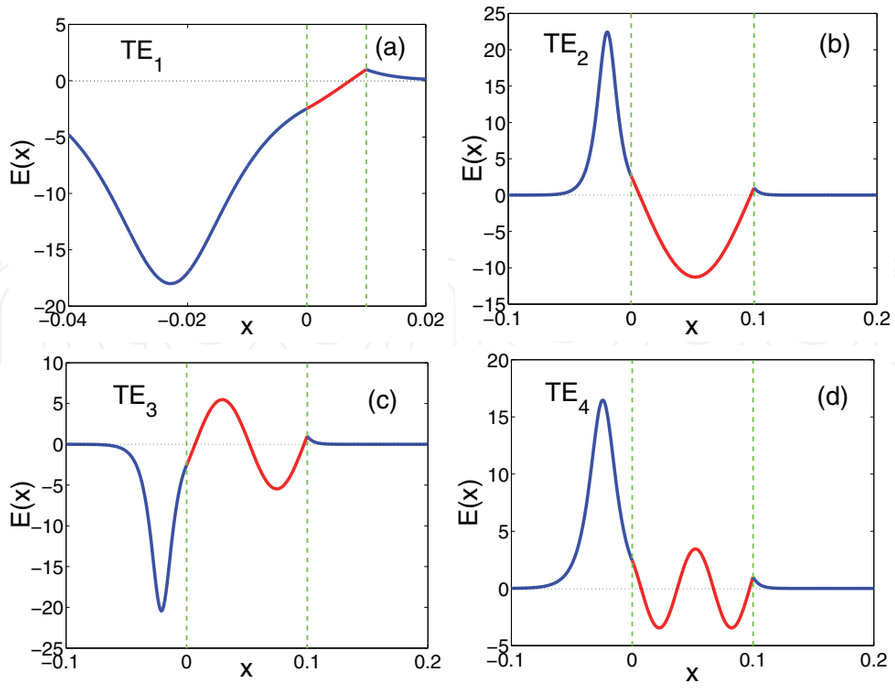

Fig. 14. (Color online) Guided modes in nonlinear NZPIM waveguide when $\omega = 0.8\omega_D < \omega_D$, $\alpha = 0.003$, $\epsilon_1^L = 1.2$ and $\epsilon_2 = 2$. (a) TE_1: $\kappa_2 d = 0.93864$, $d = 1cm$; (b) TE_2: $\kappa_2 d = 3.46529$, $d = 10cm$; (c) TE_3: $\kappa_2 d = 6.95257$, $d = 10cm$; (d) TE_4: $\kappa_2 d = 10.5005$, $d = 10cm$.

4.2 Nonlinear fast wave guided modes

Case 1: $\omega < \omega_D$, and $\epsilon_3 = \mu_3 < 0$. As shown in Fig. 14, we find that the fundamental TE_0 mode is absent for any parameters of the nonlinear NZPIM waveguide. The unique property is very different from the case of conventional nonlinear waveguide where the lowest-order TE_0 guided mode is always exist (Stegeman et al., 1984). The lowest-order guided mode of the nonlinear NZPIM waveguide is TE_1 mode, which can not coexist with higher-order guided modes for some waveguide parameters. For the TE_0 guided modes, it should satisfy the condition $k_2 d = 2\phi_{refl1} + 2\phi_{refl2}$ (Shadrivov et al., 2003; 2005; Shen et al., 2010a), where $2\phi_{refl1}$ and $2\phi_{refl2}$ are the phase retardation upon the total internal reflection at the interface between core and cladding and at the interface between core and substrate. In previous works (Shadrivov et al., 2003; 2005; Shen et al., 2010a), both $2\phi_{refl1}$ and $2\phi_{refl2}$ are negative, then the TE_0 mode does not exist. In a linear waveguide with left handed material cover, $2\phi_{refl1}$ is negative but $2\phi_{refl2}$ is positive, which may support the TE_0 mode with appropriate physical parameters. However, the nonlinear physical mechanism in this work is different from the linear dynamics (Wang et al., 2008). We emphasize that the nonlinear NZPIM waveguide can not support the TE_0 mode due to the nonlinear dispersion when the angular frequency is smaller than DP.

Case 2: $\omega > \omega_D$, and $\epsilon_3 = \mu_3 > 0$. In Fig. 15, we plot the nonlinear guided modes when the angular frequency is larger than DP. It is shown that the properties of the nonlinear NZPIM waveguide can be treated as a conventional nonlinear dielectric waveguide. From Fig. 15, we can see that the nonlinear NZPIM can support the fundamental guided mode [Fig. 15 (a)], though it can not coexist with higher-order modes within the same waveguide for general parameters. This result is different from the case that the nonlinear NZPIM waveguide can not

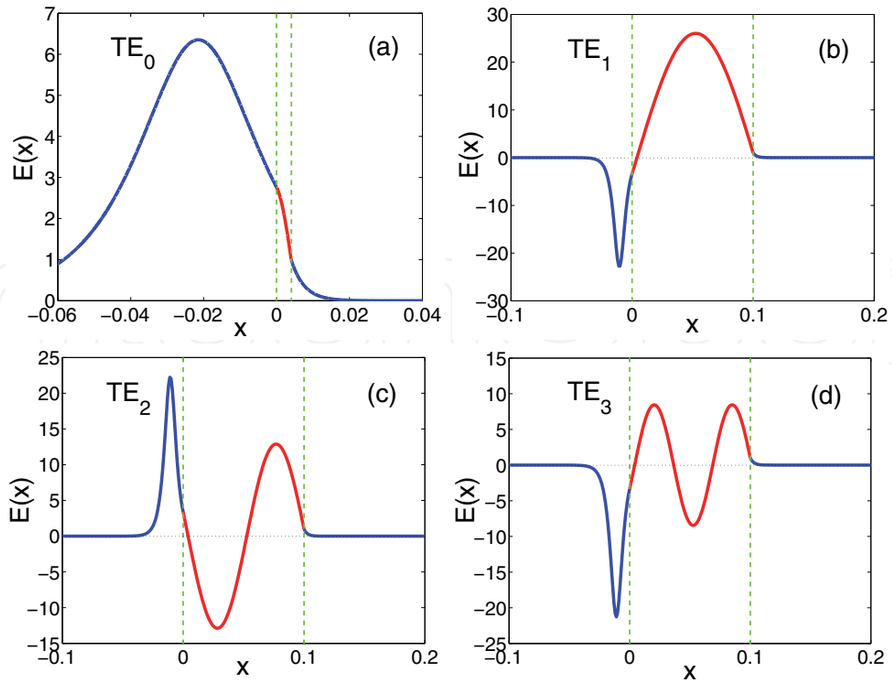

Fig. 15. (Color online) Guided modes in nonlinear NZPIM waveguide when $\omega = 4/3\omega_D > \omega_D$, $\alpha = 0.003$, $\epsilon_1^L = 1.2$ and $\epsilon_2 = 2$. (a) TE_0: $\kappa_2 d = 0.960548$, $d = 0.4cm$; (b) TE_1: $\kappa_2 d = 3.23447$, $d = 10cm$; (c) TE_2: $\kappa_2 d = 6.47046$, $d = 10cm$; (d) TE_3: $\kappa_2 d = 9.70986$, $d = 10cm$.

support the fundamental mode when the angular frequency is smaller than DP. Although the physical mechanism of nonlinear dispersion is different from the linear case, we can see that the nonlinear guided modes can also be treated as electronic wave in graphene waveguide (Zhang et al., 2009), corresponding to the Kelin tunneling (lack of fundamental mode) and classical motion (support fundamental mode), respectively.

Since the maximum of the magnitude at the interface between a nonlinear media and a linear media locates inside the nonlinear media (Shadrivov et al., 2004), the guided modes not only have mode energy in the core, but also a peak mode energy in the nonlinear substrate region, as shown in both Fig. 14 and Fig. 15. This result is identical with the conventional nonlinear waveguide (Stegeman et al., 1984).

We further show the unique properties of nonlinear guides modes near DP in the nonlinear NZPIM waveguide with the angular frequency varying from $\omega < \omega_D$ to $\omega > \omega_D$ in Fig. 16 when the nonlinearity is self-focusing [Fig. 16 (a) and (b)] and self-defocusing [Fig. 16 (c) and (d)], respectively. When the nonlinearity is self-focusing, like the behaviors of light in linear NZPIM (Chen et al., 2009; Shen et al., 2010a), there also exists an asymmetric forbidden band for the dispersion [Fig. 16 (a)] which means the nonlinear guided modes are not continuous near DP. The band will become narrower when the order of the guided modes increases which is opposite to the case that the band will become wider when the order of the guided modes increases in linear NZPIM waveguide (Shen et al., 2010a). Another important and interesting phenomenon is that the bang gap can be modulated by the strength of the nonlinearity. It is obviously that the band gap will become wider when the nonlinear index α increases [Fig. 16 (b)]. The band gap will also become wider with the increase of the wave intensity when

the nonlinear index α is fixed (not shown). However, the self-defocusing nonlinearity can eliminate the asymmetric band gap, leading to the continuation of the guided modes near DP, as shown in Fig. 16 (c) and (d). The field in the core of the NZPIM waveguide with self-defocusing nonlinearity is represented in the form of **csch** function, and its dispersion can be obtained in the same way. The tunable gap may have potential application in electron wave filters in nonlinear graphene fibre optics (Chen and Tao, 2009).

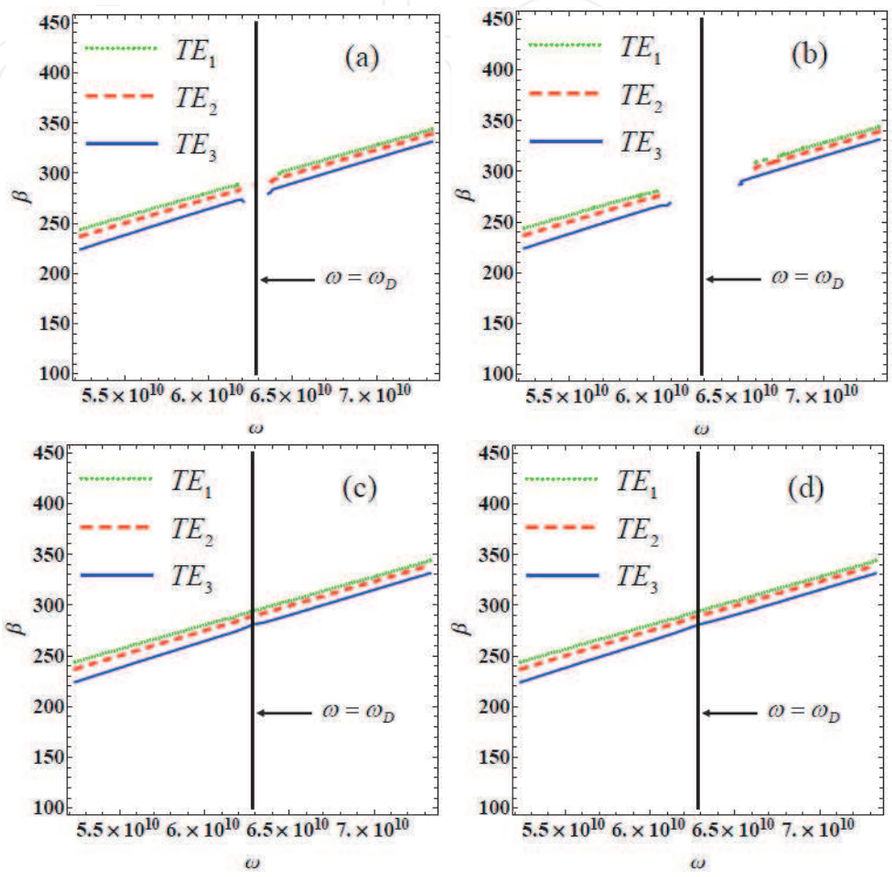

Fig. 16. (Color online) The propagation constant β versus the incident frequency ω near the DP in the nonlinear NZPIM waveguide, the core thickness is $d = 0.1$, $\epsilon_1^L = 1.2$, $\epsilon_2 = 2$, and the nonlinearity are (a) $\alpha = 0.0001$, (b) $\alpha = 0.0008$, (c) $\alpha = -0.0001$, and (d) $\alpha = -0.0008$.

4.3 Nonlinear surface guided modes

We also find that when $\omega < \omega_D$, the nonlinear NZPIM waveguide can propagate nonlinear surface guided modes-slow wave. In this case, the wave vectors in core, substrate and cladding are all imaginary. The electric fields in three regions can be written as

$$\psi(x) = \begin{cases} \frac{k_1}{k_0}\sqrt{\frac{2}{\alpha\mu_1}}\mathrm{sech}[k_1(x-x_0)], & x < 0, \\ A\cosh[k_2(x-d)] + B\sinh[k_2(x-d)], & 0 < x < d, \\ Ce^{-k_3(x-d)}, & x > d, \end{cases} \tag{38}$$

where $k_1^2 = \beta^2 - k_0^2\epsilon_1^L\mu_1$, $k_2^2 = \beta^2 - k_0^2\epsilon_2\mu_2$, and $k_3^2 = \beta^2 - [2(\omega - \omega_D)/c]^2$ are the transverse decay wave vectors in the substrate, core, and cladding, β is the propagation constant of the slow wave guided modes.
Similarly, we obtain the following dispersion relation

$$\tanh(\kappa_2 d) = -\frac{\mu_1\mu_2 k_2 k_3 - \mu_2\mu_3 k_1 k_2 \tanh(-k_1 x_0)}{\mu_1\mu_3 k_2^2 - \mu_2^2 k_1 k_3 \tanh(-k_1 x_0)}. \tag{39}$$

where $x_0 = -\frac{1}{k_1}\mathrm{sech}^{-1}\left[\frac{k_0}{k_1}\sqrt{\frac{\alpha\mu_1}{2}}(\cosh k_2 d + \frac{\mu_2 k_3}{\mu_3 k_2}\sinh k_2 d)C\right]$ is the position of the maximum of the amplitude in nonlinear substrate, C being the amplitude of the electric field at the interface $x = d$.

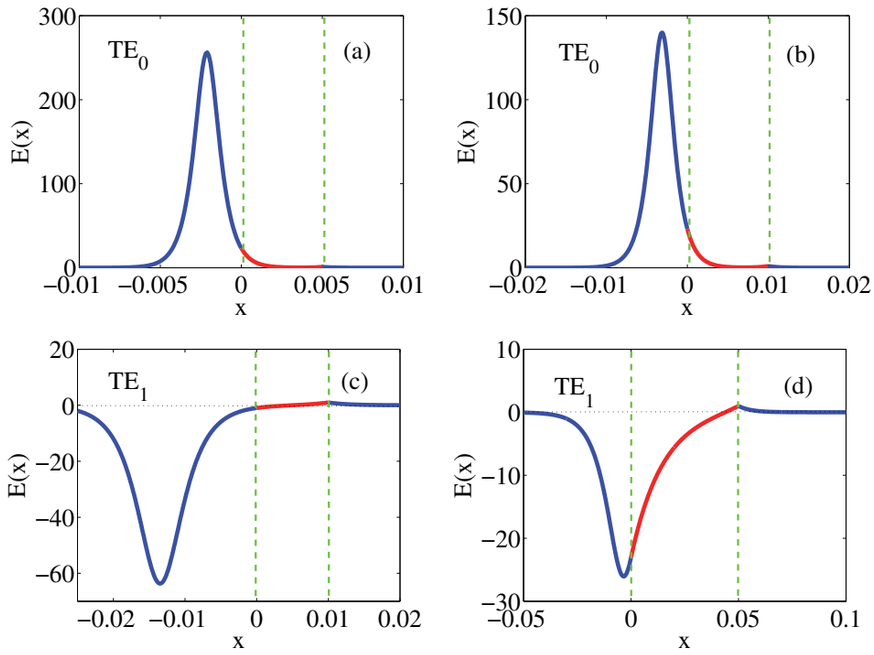

Fig. 17. (Color online) Slow wave guided modes in nonlinear NZPIM waveguide when $\omega = 0.7\omega_D < \omega_D$, the nonlinearity is $\alpha = 0.003$, $\epsilon_1^L = 1.2$, $\epsilon_2 = 2$. (a) TE_0: $\kappa_2 d = 7.25054$, $d = 0.5cm$; (b) TE_0: $\kappa_2 d = 7.8406$, $d = 1cm$; (c) TE_1: $\kappa_2 d = 3.36844$, $d = 1cm$; (d) TE_1: $\kappa_2 d = 3.42543$, $d = 5cm$.

We plot the nonlinear slow waves guided modes in Fig. 17. We find that only the lowest order even (TE_0) or odd (TE_1) surface guided modes can exist in the nonlinear NZPIM waveguide which crucially depend on the physical parameters. When the core thickness is smaller, the waveguide can only support TE_0 mode surface wave [Fig. 17 (a)]. When the core thickness getting bigger, the waveguide can support both the TE_0 mode and the TE_1 mode surface waves [Fig. 17 (b) and (c)]. However, when the core thickness is larger, the waveguide can only support the TE_1 mode surface wave[Fig. 17 (d)]. Recent research showed that the optically discrete and surface solitons in honeycomb photonic lattices can be regarded as an optical analog of graphene nanoribbons (Molina and Kivshar, 2010). Surface solitons (Savin and Kivshar, 2010a) and vibrational Tamm states (Savin and Kivshar, 2010b) at the edges of graphene nanoribbons have also been reported recently. We hope that our results

obtained here may also predict the nonlinear surface mode of electrons and holes in nonlinear graphene waveguide.

5. Further work on optical DP in NZPIM

In the recent years, graphene supperlatices with periodic potential structures has drawn considerable attention due to the fact that superlattices are very successful in controlling the electronic structures of many conventional semiconducting materials (Tsu, 2005). Many theoretical (Park et al., 2008a;b) and experimental (Sutter et al., 2008) works have been focus on the devices of graphene-based superlattices. Wang *et al.* have presented the result on a new DP which is exactly located at the energy which corresponds to the zero-averaged wavenumber inside the one-dimensional (1D) periodic potentials (Wang and Zhu, 2010a; Wang and Chen, 2011). The gap for the zero-averaged wavenumber is quite different from the Bragg gap, which is analogous to the case of the one-dimensional PCs containing left-handed and right-handed materials (Bliokh et al., 2009; Wang and Zhu, 2010b).

Based on the rapid developments in both theoretical and experimental works on graphene-based superlattices, and the analogy phenomena between electron waves in graphene and optics in NZPIM, the optical propagation in one-dimensional PCs containing NZPIM will be an interesting and challenge task in the future. We will study the transmission of optics through an one-dimensional PCs containing NZPIM, and predict some novel properties, such as Goos-Hänchen shifts (Chen et al., 2009), zero-averaged index gap (Wang and Zhu, 2010b), new Dirac gap, and Bragg gap etc. The propagation of one-dimensional NZPIM PCs containing a nonlinear defect will be another significative question as well.

6. Conclusion

In summary, we have investigated the nonlinear plasmonics in NZPIM and shown that the dynamics of electron wave in graphene can be simulated by the analogy of optics in NZPIM. The unique propagation of optics near the DP in NZPIM, such as frequency threshold of nonlinear surface waves, and tunable band gap of the nonlinear guided modes, will lead to the potential applications in guided wave optics, integral optics and optical-based devices. Our results will also give the deeper understanding of several exotic phenomena in graphene. We hope our work will motivate the further work to simulate and predict many exotic phenomena in graphene with relatively simple optical experiments.

7. Acknowledgement

The authors appreciate L.-G. Wang and X. Chen for their pioneering and enlightening works on optical DP in NZPIM. This work is supported by the Chinese National Natural Science Foundation (Grant No. 60808002) and the Shanghai Leading Academic Discipline Project (Grant No. S30105).

8. References

Ablowitz, M. J.; Nixon, S. D. & Zhu, Y. (2009). Conical diffraction in honeycomb lattices. *Phys. Rev. A*, Vol. 79, No. 5, May -2009, 053830 (1-6), ISSN 1050-2947

Bahat-Treidel, O.; Peleg, O. & Segev, M. (2008). Symmetry breaking in honeycomb photonic lattices. *Opt. Lett.*, Vol. 33, No. 19, Sep -2008, 2251-2253, ISSN 0146-9592

Bahat-Treidel, O.; Peleg, O.; Grobman, M.; Shapira, N. & Segev, M. (2010). Klein tunneling in deformed honeycomb lattices. *Phys. Rev. Lett.*, Vol. 104, No. 6, Feb -2010, 063901 (1-4), ISSN 0031-9007

Bahat-Treidel, O.; Peleg, O.; Segev, M. & Buljan, H. (2010). Breakdown of Dirac dynamics in honeycomb lattices due to nonlinear interactions. *Phys. Rev. A*, Vol. 82, No. 1, Jul -2010, 013830 (1-6), ISSN 1050-2947

Beenakker, C. W. (2008). Colloquium: Andreev reflection and Klein tunneling in graphene.*Rev. Mod. Phys.*, Vol. 80, No. 4, Oct -2008, 1337-1354, ISSN 0034-6861

Beenakker, C. W. J.; Sepkhanov, R. A.; Akhmerov, A. R. & Tworzydlo, J. (2009). Quantum Goos-Hänchen effect in graphene. *Phys. Rev. Lett.*, Vol. 102, No. 14, Jan -2009, 146804 (1-4), ISSN 0031-9007

Bliokh, Y. P.; Freilikher, V.; Savel'ev, S. & Nori, F. (2009). Transport and localization in periodic and disordered graphene superlattices. *Phys. Rev. B*, Vol. 79, No. 7, Feb -2009, 075123 (1-4), ISSN 1098-0121

Castro Neto, A. H.; Guinea, F.; Peres, N. M. R.; Novoselov, K. S. & Geim, A. K. (2009). The electronic properties of graphene. *Rev. Mod. Phys.*, Vol. 81, No. 1, Jan -2009, 109ÍC162, ISSN 0034-6861

Cheianov, V. V.; Fal'ko, V. & Altshuler, B. L. (2007). The focusing of electron flow and a veselago lens in graphene p-n junctions. *Science*, Vol. 315, No. 5816, Mar -2007, 1252-1255, ISSN 0036-8075

Chen, X. & Tao, J.-W. (2009). Design of electron wave filters in monolayer graphene by tunable transmission gap. *Appl. Phys. Lett.*, Vol. 94, No. 26, Jun -2009, 262102 (1-3), ISSN 0003-6951

Chen, X.; Wang, L.-G. & Li, C.-F. (2009). Transmission gap, Bragg-like reflection, and Goos-Hänchen shifts near the Dirac point inside a negative-zero-positive index metamaterial slab. *Phys. Rev. A*, Vol. 80, No. 4, Oct -2009, 043839 (1-5), ISSN 1050-2947

Chen, X.; Wei, R.-R.; Shen, M.; Zhang Z.-F. & Li, C.-F. (2010). Bistable and negative lateral shifts of the reflected light beam from Kretschmann configuration with nonlinear left-handed metamaterials. *Appl. Phys. B*, Vol. 101, No. 1-2, May -2010, 283-289, ISSN 0946-2171

Darancet, P.; Olevano, V. & Mayou, D. (2009). Coherent electronic transport through graphene constrictions: Subwavelength regime and optical analogy. *Phys. Rev. Lett.*, Vol. 102, No. 13, Mar -2009, 136803 (1-4), ISSN 0031-9007

Ghosh, S. & Sharma, M. (2009). Electron optics with magnetic vector potential barriers in graphene. *J. Phys.: Condens. Matter*, Vol. 21, No. 29, Jul -2009, 292204 (1-8), ISSN 0953-8984

Güney D. Ö. & Meyer, D. A. (2009). Negative refraction gives rise to the Klein paradox. *Phys. Rev. A*, Vol. 79, No. 6, Jun -2009, 063834 (1-4), ISSN 1050-2947

Haddad L. H. & Carr, L. D. (2009). The nonlinear Dirac equation in Bose-Einstein condensates: Foundation and symmetries. *Phys. D*, Vol. 238, No. 15, Jul -2009, 1413-1421, ISSN 0167-2789

Hendry, E.; Hale, P. J.; Moger, J.; Savchenko, A. K. & Mikhailov, S. A. (2010). Coherent Nonlinear Optical Response of Graphene. *Phys. Rev. Lett.*, Vol. 105, No. 9, Aug -2010, 097401 (1-4), ISSN 0031-9007

Katsnelson, M. I.; Novoselov, K. S. & Geim, A. K. (2006). Chiral tunnelling and the Klein paradox in graphene. *Nature Physics*, Vol. 2, Feb -2006, 620-625, ISSN 1745-2473

Kivshar, Y. S. (2008). Nonlinear optics: The next decade. *Opt. Exp.*, Vol.16, No. 26, Dec-2008, 22126-22128, ISSN 1094-4087

Mikhailov, S. A. (2007). Non-linear electromagnetic response of graphene. *Europhys. Lett.*, Vol. 79, No. 2, Jul -2007, 27002 (1-4), ISSN 0295-5075

Molina, M. I. & Kivshar, Y. S. (2010). Discrete and surface solitons in photonic graphene nanoribbons. *Opt. Lett.*, Vol. 35, No. 17, Sep -2010, 2895-2897, ISSN 0146-9592

Novoselov, K. S.; Geim, A. K.; Morozov, S. V.; Jiang, D.; Zhang, Y.; Dubonos, S. V.; Grigorieva, I. V. & Firsov, A. A.(2004). Electric field effect in atomically thin carbon films. *Science*, Vol. 306, No. 5696, Oct -2004, 666-669, ISSN 0036-8075

Novoselov, K. S.; Geim, A. K.; Morozov, S. V.; Grigorieva, I. V.; Dubonos, S. V. & Firsov, A. A. (2005). Two-dimensional gas of massless Dirac fermions in graphene. *Nature (London)*, Vol. 438, Nov -2005, 197-200, ISSN 0028-0836

Park, C.-H.; Yang, L.; Son, Y.-W.; Cohen, M. L. & Louie, S. G. (2008). Electron beam supercollimation in graphene superlattices. *Nano Lett.*, Vol. 8, No. 9, Aug -2008, 2920-2924, ISSN 1530-6984

Park, C.-H.; Yang, L.; Son, Y.-W.; Cohen, M. L. & Louie, S. G. (2008). Anisotropic behaviours of massless Dirac fermions in graphene under periodic potentials. *Nature Physics*, Vol. 4, No. 3, Feb -2008, 213-217, ISSN 1745- 2473

Peleg, O.; Bartal, G.; Freedman,B.; Manela, O.; Segev, M. & Christodoulides, D. N. (2007). Conical diffraction and gap solitons in honeycomb photonic lattices. *Phys. Rev. Lett.*, Vol. 98, No. 10, Mar -2007, 103901 (1-4), ISSN 0031-9007

Ruppin, R. (2000). Surface polaritons of a left-handed medium. *Phys. Lett. A*, Vol. 277, No. 1, Nov -2000, 61-64, ISSN 0375-9601

Savin, A. V. & Kivshar, Y. S. (2010). Surface solitons at the edges of graphene nanoribbons. *Europhys. Lett.*, Vol. 89, No. 4, Mar -2010, 46001 (1-6), ISSN 0295-5075

Savin, A. V. & Kivshar, Y. S. (2010). Vibrational Tamm states at the edges of graphene nanoribbons. *Phys. Rev. B*, Vol. 81, No. 16, Apr -2010, 165418 (1-9) , ISSN 1098-0121

Shadrivov, I. V.; Sukhorukov, A. A. & Kivshar, Y. S. (2003). Guided modes in negative-refractive-index waveguides. *Phys. Rev. E*, Vol. 67, No. 5, May -2003, 057602 (1-4), ISSN 1539-3755

Shadrivov, I. V.; Sukhorukov, A. A.; Kivshar, Y. S.; Zharov, A. A.; Boardman, A. D. & Egan, P. (2004). Nonlinear surface waves in left-handed materials. *Phys. Rev. E*, Vol. 69, No. 1, Jan -2004, 016617 (1-9), ISSN 1539-3755

Shadrivov, I. V.; Sukhorukov, A. A. & Kivshar, Y. S. (2005). Complete band gaps in one-dimensional left-handed periodic structures. *Phys. Rev. Lett.*, Vol. 95, No. 19, Nov -2005, 193903 (1-4), ISSN 0031-9007

Shen, M.; Ruan, L.-X. & Chen, X. (2010). Guided modes near the Dirac point in negative-zero-positive index metamaterial waveguide. *Opt. Exp.*, Vol. 18, No. 12, May -2010, 12779-12787, ISSN 1094-4087

Shen, M.; Ruan, L.-X.; Chen, X.; Shi, J.-L.; Ding, H.-X.; Xi, N. & Wang Q. (2010). Nonlinear surface waves near the Dirac point in negative-zero-positive index metamaterial. *J. of Opt.*, Vol. 12, N, 8, Aug- 2010, 085201 (1-5), ISSN 2040-8978

Shen, M.; Ruan, L.-X.; Wang, X.-L; Shi, J.-L. & Wang Q. (2011). Tunable band gap near the Dirac point in nonlinear negative-zero-positive index metamaterial waveguide. *Phys. Rev. A*, (accepted), ISSN 1050-2947

Smith, D. R.; Padilla W. J., Vier, D. C.; Nemat-Nasser, S. C. & Schultz, S. (2000). Composite Medium with Simultaneously Negative Permeability and Permittivity. *Phys. Rev. Lett.*, Vol. 84, No. 18, 4184-4187, May-2000, ISSN 0031-9007

Sepkhanov, R. A.; Bazaliy, Y. B. & Beenakker, C. W. J. (2007). Extremal transmission at the Dirac point of a photonic band structure. *Phys. Rev. A*, Vol. 75, No. 6, Jun -2007, 063813 (1-5), ISSN 1050-2947

Stegeman, G. I.; Seaton, C. T.; Chilwell, J. & Smith, S. D. (1984). Nonlinear waves guided by thin films. *Appl. Phys. Lett.*, Vol. 44, No. 9, May -1984, 830-832, ISSN 0003-6951

Sutter, P. W.; Flege, J. I. & Sutter, E. A. (2008). Epitaxial graphene on ruthenium. *Nature Materials*, Vol. 7, No. 5, May -2008, 406-411, ISSN 1476-1122

Tsakmakidis, K. L.; Boardman, A. D. & Hess, O. (2007). 'Trapped rainbow' storage of light in metamaterials. *Nature (London)*, Vol. 440, Nov -2007, 397-401, ISSN 0028-0836

Tsu, R. (2005), Superlattice to Nanoelectronics, Elsevier, ISBN: 978-0-08-044377-5, Oxford.

Wang, L.-G.; Wang, Z.-G.; Zhang, J.-X. & Zhu, S.-Y. (2009). Realization of Dirac point with double cones in optics. *Opt. Lett.*, Vol. 34, No. 10, May -2009, 1510-1512, ISSN 0146-9592

Wang, L.-G.; Wang, Z.-G. & Zhu, S.-Y. (2009). Zitterbewegung of optical pulses near the Dirac point inside a negative-zero-positive index metamaterial. *Europhys. Lett.*, Vol. 86, No. 4, Jun -2009, 47008 (1-5), ISSN 0295-5075

Wang, L.-G.; Li, G.-X. & Zhu, S.-Y. (2010). Thermal emission from layered structures containing a negative-zero-positive index metamaterial. *Phys. Rev. B*, Vol. 81, No. 7, Jan -2010, 073105 (1-4) , ISSN 1098-0121

Wang, L.-G. & Zhu, S.-Y. (2010). Electronic band gaps and transport properties in graphene superlattices with one-dimensional periodic potentials of square barriers. *Phys. Rev. B*, Vol. 81, No. 20, May -2010, 205444 (1-9), ISSN 1098-0121

Wang, L.-G. & Zhu, S.-Y. (2010), The reversibility of the Goos-Hänchen shift near the band- crossing structure of one-dimensional photonic crystals containing left-handed metamaterials. *Appl. Phys. B: Lasers and Optics*, Vol.98, No. 2-3, Feb.-2010, 459-463, ISSN 0946-2171

Wang, L.-G. & Chen, X. (2011). Robust zero-averaged wave-number gap inside gapped graphene superlattices. *J. Appl. Phys.*, Vol.109, No.3, Feb.-2011, 033710 (1-8), ISSN 0021-8979

Wang, Q. & Awai, I. (1998). Frequency characteristics of the magnetic spatial solitons on the surface of an antiferromagnet. *J. Appl. Phys.*, Vol.83, No.1, Jan.-1998, 382-387, ISSN 0021-8979

Wang, Z.-H.; Xiao, Z.-Y. & Li, S. P. (2008). Guided modes in slab waveguides with a left handed material cover or substrate. *Opt. Commun.*, Vol.281, No.4, Feb.-2008, 607-613, ISSN 0030-4018

Williams, J. R.; Low, Tony; Lundstrom, M. S. & Marcus C. M. (2011). Gate-controlled guiding of electrons in graphene. *Nature Nanotechnology*, Vol.281, No.4, Apr-2011, 222-225, ISSN 1748-3387

Wu, X. (2011). Electronic fiber in graphene. *Appl. Phys. Lett.*, Vol. 98, No. 8, Feb -2011, 082117 (1-3), ISSN 0003-6951

Xu, G.-D.; Pan, T.; Zang, T.-C. & Sun, J. (2009). Nonlinear surface polaritons in anisotropic Kerr-type metamaterials. *J. Phys. D: Appl. Phys.*, Vol. 42, No. 4, Jan -2009, 045303 (1-7), ISSN 1361-6463

Zhao, L. & Yelin, S. F. (2010). Proposal for graphene-based coherent buffers and memories. *Phys. Rev. B*, Vol. 81, No. 11, Mar -2010, 115441 (1-4), ISSN 1098-0121

Zhang, Y.; Tan, Y.-W.; Stormer, H. L. & Kim, P. (2005). Experimental observation of the quantum Hall effect and Berry's phase in graphene. *Nature (London)*, Vol. 438, Nov -2005, 201-204, ISSN 0028-0836

Zhang, X. (2008). Observing Zitterbewegung for photons near the Dirac point of a two-dimensional photonic crystal. *Phys. Rev. Lett.*, Vol. 100, No. 11, Mar -2008, 113903 (1-4), ISSN 0031-9007

Zhang, F.-M.; He, Y. & Chen, X. (2009). Guided modes in graphene waveguides. *Appl. Phys. Lett.*, Vol. 94, No. 21, May -2009, 212105 (1-3), ISSN 0003-6951

Ziolkowski, R. W. (2004). Propagation in and scattering from a matched metamaterial having a zero index of refraction. *Phys. Rev. E*, Vol. 70, No. 4, Oct -2004, 046608 (1-12), ISSN 1539-3755

IntechOpen

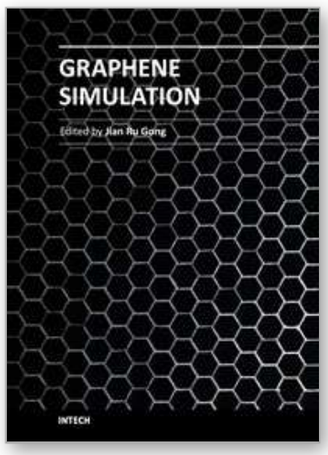

Graphene Simulation

Edited by Prof. Jian Gong

ISBN 978-953-307-556-3
Hard cover, 376 pages
Publisher InTech
Published online 01, August, 2011
Published in print edition August, 2011

Graphene, a conceptually new class of materials in condensed-matter physics, has been the interest of many theoretical studies due to the extraordinary thermal, mechanical and electrical properties for a long time. This book is a collection of the recent theoretical work on graphene from many experts, and will help readers to have a thorough and deep understanding in this fast developing field.

How to reference

In order to correctly reference this scholarly work, feel free to copy and paste the following:

Ming Shen and Linxu Ruan (2011). Nonlinear Plasmonics Near the Dirac Point in Negative-Zero-Positive Index Metamaterials–Optical Simulations of Electron in Graphene, Graphene Simulation, Prof. Jian Gong (Ed.), ISBN: 978-953-307-556-3, InTech, Available from: http://www.intechopen.com/books/graphene-simulation/nonlinear-plasmonics-near-the-dirac-point-in-negative-zero-positive-index-metamaterials-optical-simu

INTECH
open science | open minds

InTech Europe
University Campus STeP Ri
Slavka Krautzeka 83/A
51000 Rijeka, Croatia
Phone: +385 (51) 770 447
Fax: +385 (51) 686 166
www.intechopen.com

InTech China
Unit 405, Office Block, Hotel Equatorial Shanghai
No.65, Yan An Road (West), Shanghai, 200040, China
中国上海市延安西路65号上海国际贵都大饭店办公楼405单元
Phone: +86-21-62489820
Fax: +86-21-62489821

© 2011 The Author(s). Licensee IntechOpen. This chapter is distributed under the terms of the Creative Commons Attribution-NonCommercial-ShareAlike-3.0 License, which permits use, distribution and reproduction for non-commercial purposes, provided the original is properly cited and derivative works building on this content are distributed under the same license.

IntechOpen

IntechOpen